Arab J Geosci (2015) 8:2551–2565
DOI 10.1007/s12517-014-1349-3

ORIGINAL PAPER

Carbonate diagenesis of the mixed clastic–carbonate Galala Formation, North Eastern Desert, Egypt

Mohamed S. Abu El Ghar · M. A. Khalifa · A. W. Hussein

Received: 29 September 2013 / Accepted: 19 February 2014 / Published online: 13 April 2014

Abstract The carbonate diagenetic history of the Late Cenomanian Galala Formation (North Eastern Desert, Egypt) successively includes marine–phreatic, mixed marine–meteoric, meteoric–phreatic, and subaerial diagenesis. The marine–phreatic diagenesis proceeded through the following path: (a) micritization of skeletal allochems; (b) shallow marine cementation (fibrous calcite and circumgranular spar cements); and (c) dolomitization of the lime mud to fine-crystalline dolostone (dolomicrite). The mixing marine–meteoric diagenesis was associated with the formation of the coarse-crystalline dolostone (dolosparite) by the aggrading recrystallization of the precursor dolomicrite. The meteoric–phreatic diagenesis comprises of the following consecutive stages: (a) the development of granular calcite, blocky calcite, and syntaxial rim cements; and (b) the recrystallization of both the carbonate matrix and bioclasts. The subaerial diagenesis is responsible for the calcitization of the precursor dolomites; whereas, the percolation of meteoric water results in the removal of the Mg ions from the dolostone and the production of calcite.

Keywords Carbonate diagenesis · Galala · Eastern Desert · Egypt

M. S. Abu El Ghar (✉) · A. W. Hussein
Geology Department, Faculty of Science, Fayoum University, 63514, Fayoum, Egypt
e-mail: msa02@fayoum.edu.eg

M. S. Abu El Ghar
e-mail: mohamedabuelghar@yahoo.com

M. A. Khalifa
Geology Department, Faculty of Science, Menuofia University, Shebein El-Kom, Egypt

Introduction

The Cretaceous of Egypt includes eight facies belts (Sinai, Ataqa, Southern Galala, Wadi Qena, Nile Valley, Nubia-Abu Ballas, Farafra-Bahariya, and North Western Desert; Issawi and Osman 2000). The Galala Formation (Late Cenomanian) is one of the most conspicuous rock units of the Cretaceous stratigraphic sequence of the Egyptian territory. It is outcropped within both Ataqa and Southern Galala facies belts of Issawi and Osman (op.cit). The carbonates of the Galala Formation are characterized by their cyclic nature of sedimentation, besides their richness in the Cenomanian macrofauna (i.e., oysters, gastropods, ammonites, and echinoderms).

The majority of previous studies on the Galala Formation were concentrated on its stratigraphy and paleontology. Few workers attended with the digenetic history of Galala Formation (e.g., Mohammad and Omran 1992; Abu El-Hassan 1997; Khalil and Mostafa 2001; Mostafa and Hassan 2003; Essa 2005). The intention of this work is to describe and to discuss the main post-depositional changes that acted upon limestones and dolostones in order to deduce the carbonate diagenetic history of the Galala Formation.

The Galala Formation unconformably overlies the fluvial to fluvio-marine sediments of the Aptian–Albian Malha Formation. The unconformity is represented by the paleosol horizons at Gebel El-Zeit and the Southern Galala and by the intraformational conglomerates at Gebel Shabraweet. It is unconformably overlaid by the El-Khashm Formation at Gebel El-Zeit, the Northern Galala, and the Gebel Ataqa. The unconformity is delineated by the presence of undulated caliche zone. The Wata Formation is paraconformably overlying the Galala Formation at the Southern Galala. At Gebel Shabraweet, the Galala Formation unconformably underlies the Maghra El-Hadida Formation. The contact is taken at the top of the cherty dolostone of the uppermost part of the Galala Formation. The lithostratigraphic classification of the studied succession is given in Table 1. The litho-, bio-, and petrofacies of the Galala Formation reflect a shallow ramp depositional model (Hussein 2010). The main characteristics of the Galala Formation and its proposed depositional environments are highlighted in Table 2.

Methods

To accomplish the target of this study, the following steps were executed: (a) a detailed field work was carried out, including measuring, describing, sampling, and constructing lithostratigraphic logs in order to define the boundaries between the rock units of five representative outcrops covering the study area from south to north; Gebel El-Zeit, the Southern Galala, the Northern Galala, Gebel Ataqa, and Gebel Shabraweet (Fig. 1). (b) About 200 thin sections of the carbonate rocks have been prepared and examined under a polarized microscope. Selected carbonate thin sections were stained with Alizarin Red-S and Potassium Ferricyanide following the method outlined by Dickson (1966), in order to distinguish between different carbonate minerals and the ferroan and non-ferroan dolomite. (c) Scanning electron microscopy (SEM) was used to detect the microscopic textural and diagenetic features of 25 samples. It was carried out in the Central Laboratories Sector of the Egyptian Geological Survey and Mining Authority using SEM Model Philips XL 30 attached with EDX unit with accelerating voltage 30 kV and resolution for W. (3.5 nm). The samples were coated with gold. (d) Chemical analyses on 20 powdered rock samples; their compositions, expressed as % in major oxides (CaO, MgO, Fe_2O_3, and Al_2O_3) and as ppm in trace elements (Sr and Na), are important for understanding the chemistry of the studied rocks. These chemical analyses were carried out in the laboratories of the Nuclear Materials Authority and the Central Laboratories Sector of the Egyptian Geological Survey and Mining Authority. The measurements of the major oxides were done by two methods. The first method follows the method of Shapiro and Brannock (1962) with the modification of El-Reedy (1984). The samples were opened as two solutions (A and B). The solution A was used for the determination of Al_2O_3, using spectrophotometer technique. On the other hand, the solution B was used for the determination of CaO, MgO, and Fe_2O_3, using the titrimetric methods, and Na_2O, using the flame photometric methods. The second method was done; whereas, the XRF analysis was carried out for powder (200 μ) samples using a Philips X-Ray Fluorescence equipment model PW/1404, with Rh radiation tube and four analyzing crystals. Crystal (LIF-200) was used for determining Ca and Fe, while crystal (TIAP) was used to estimate Mg and Na. Crystal (PET) was used for determining Al. The concentration of the analyzed elements was determined by using the software Kernal X-40 with an accuracy of 99.5 % and a confidence limit of 95.6 %. The estimation of the major elements were done as powder pellets, which were prepared by pressing the powder of the sample in Aluminium cup using Herzog presser and a 10-ton pressure. The X-ray fluorescence technique (XRF) was used to determine the trace elements using PHILIPS X'Unique-II spectrometer. The trace elements were measured by calibrating the system under the conditions

Table 1 Litostratigraphic classification of the studied sequence of the Galala Formation

<table>
<tr><th colspan="2">Section / Age</th><th>Gebel El-Zeit (section no.1)</th><th>Southern Galala (section no.2)</th><th>Northern Galala (section no.3)</th><th>Gebel Ataqa (section no.4)</th><th>Gebel Shabraweet (section no.5)</th></tr>
<tr><td rowspan="3">Late Cretaceous</td><td>Turonian-Santonian</td><td>Wata Formation</td><td>Wata Formation</td><td>Maghra El-Hadida Formation</td><td>Maghra El-Hadida Formation</td><td>Maghra El-Hadida Formation</td></tr>
<tr><td rowspan="2">Cenomanian</td><td>El-Khashm Formation</td><td rowspan="2">Galala Formation</td><td>El-Khashm Formation</td><td>El-Khashm Formation</td><td rowspan="2">Galala Formation</td></tr>
<tr><td>Galala Formation</td><td>Galala Formation</td><td>Galala Formation</td></tr>
<tr><td colspan="2">Early Cretaceous</td><td>Malha Formation</td><td>Malha Formation</td><td>Malha Formation</td><td></td><td>Malha Formation</td></tr>
</table>

Table 2 Main characteristics of the Galala Formation and the suggested depositional environments

Studied section	Lithology	Sedimentary structures	Allochemes		Orthochemes	Facies associations	Depositional environment
			Skeletal	Non-skeletal			
G. El-Zeit	-Claystone (41.6 %)	-Burrows (vertical and oblique)	-Bivalvia (Oysters)	-Glauconite pellets	-Micrite	Clastics: Claystone, sandy claystone, glauconitic claystone, sandy glauconitic siltstone, ferr. qz arenite, dol. qz arenite, siliceous qz arenite, evaporitic qz arenite, glauconitic dolomitic litharenite and paleosol (rooted ferruginous sub litharenite).	Shoreface to peritidal
	-Sandstone (33 %)	Bioturbation	-Plant remains	-Detrital quartz	-Dolomitic cement		INNER RAMP
	-Dolostone (19.8 %)	-Flaser bedding	-Phospahtic bioclasts		-Evap. cement		
	-Limestone (2.5 %)	-Cross bedding			-Ferr. cement		
	-Siltstone (1.5 %)	-Lenticular bedding			-Siliceous cement		
	-Marl. (1.1 %)	-Thin laminations					
	-Gypsum (0.5 %)	-Cross laminations					
		-Fissility in claystone					
The Southern Galala	-Claystone (82.6 %)	-Cross bedding and ripple marks in sandstones	-Bivalvia (Oysters)	-Peloids	-Micrite	Clastics: Oyster claystone, glauconitic sandy oyster claystone, ferruginous qz arenite and sandy dolomitic glauco-arenite.	
	-Dol. L.S. (6.8 %)		-Plank. forams	-Algal oncolites	-Dolomitic cement	Carbonates: Bioclastic foraminiferal wackestone, foraminiferal molluscan packstone, oncolitic packstone, dolomitic algal bioclastic packstone, dolomitic peloidal packstone and ferroan dolomicrite.	Shallow subtidal
	-Limestone (6.5 %)		-Echinoderms	-Detrital quartz	-Ferr. cement		*INTRA-RAMP BASIN*
	-Sandstone (2 %)		-Green algae	-Detrital glauconite pellets			MID RAMP
	-Glauco-arenite (1.3 %)		-Gastropods				
	-Dolostone (0.9 %)		-Ostracods				
			-Cephalopods				
			-Phospahtic bioclasts				
The Northern Galala	-Claystone (53 %)	-Burrows (vertical and oblique)	-Bivalvia (Oysters)	-Intraclasts	-Micrite	Clastics: Claystone, oyster claystone and sandy glauconitic siltstone.	Peritidal to open marine shallow subtidal
	-Dolostone (18 %)	-Thin laminations	-Echinoderms	-Oolites		Carbonates: Fossiliferous marl, caliche, lime mudstone, bioclastic foraminiferal wackestone, dolomitic molluscan wackestone, foraminiferal molluscan packstone, ostracoda molluscan packstone, sandy dolomicrite and dolomicrite.	MID RAMP
	-Limestone (12 %)	-Fissility in claystone	-Plank. forams	-Aggregates			
	-Dol. L.S (7.4 %)	-Nodular claystone	-Gastropods	-Detrital quartz			
	-Marl (6.7 %)		-Ostracods	-Detrital glauconite pellets			
	-Siltstone (3 %)		-Green algae				
			-Phospahtic bioclasts				
			-Bryozoa				
G. Ataqa	-Dolostone (39.5 %)		-Bivalvia (Oysters)	-Intraclasts	-Micrite	Clastics: Claystone.	Peritidal to shallow subtidal

Table 2 (continued)

Studied section	Lithology	Sedimentary structures	Allochemes		Orthochemes	Facies associations	Depositional environment
			Skeletal	Non-skeletal			
		-Burrows (vertical and oblique)					
	-Dol. L.S (31 %)	-Thin laminations	-Green algae	-Peloids		Carbonates: Fossiliferous marl, caliche, lime mudstone, dolomitic lime mudstone, dol. lithoclastic lime mudstone, algal bioclastic wackestone, dolomitic molluscan wackestone, dolomitic algal bioclastic packstone, dolomicrite, birds eye dolomicrite and dolosparite.	*CARBONATE BUILDUP*
	-Limestone (26 %)	-Fissility in claystone	-Echinoderms				MID RAMP
	-Claystone (2.2 %)	Bioturbation	-Gastropods				
	-Marl (1.3 %)		-Ostracods				
			-Lithoclasts				
Gebel Shabraweet	-Dolostone (51 %)	-Burrows (vertical, horizontal and oblique)	-Bivalvia (Oysters)	-Intraclasts	-Micrite	Clastics: Claystone, oyster claystone, dolomitized claystone and sandy dolomitic glauco-arenite	Peritidal to shallow subtidal
	-Limestone (19 %)	-Thin laminations	-Gastropods	-Oolites	-Fibrous calcite cement	Carbonates: Lime mudstone, dolomitic lime mudstone, molluscan-echinoidal wackestone, dol. echinoidal wackestone, dol. molluscan wackestone, molluscan peloidal packstone, oolitic peloidal grainstone, peloidal echinoidal grainstone, dolomicrite, sandy dolomicrite, ferroan dolomicrite, siliceous ferroan dolomicrite and dolosparite.	MID RAMP
	-Claystone (18 %)	-Thick-bedded	-Echninoderms	-Peloids	-Isopachous clacite cement		
	-Dol. L.S (11.9 %)	-Mud cracks	-Green algae	-Aggregates	-Granular calcite cement		
	-Glauco-arenite (0.1 %)	-Fissility in claystone	-Ostracods	-Detrital quartz			
		-Bioturbation	-Benthonic forams (Orbitoides)	-Detrital glauconite pellets			
		-Nodular claystone	-Micritized forams (benthonics)				
		-Slump structure	-Miliolids				
			-Bryozoa				
			-Phospahtic bioclasts				
			-Lithoclasts				

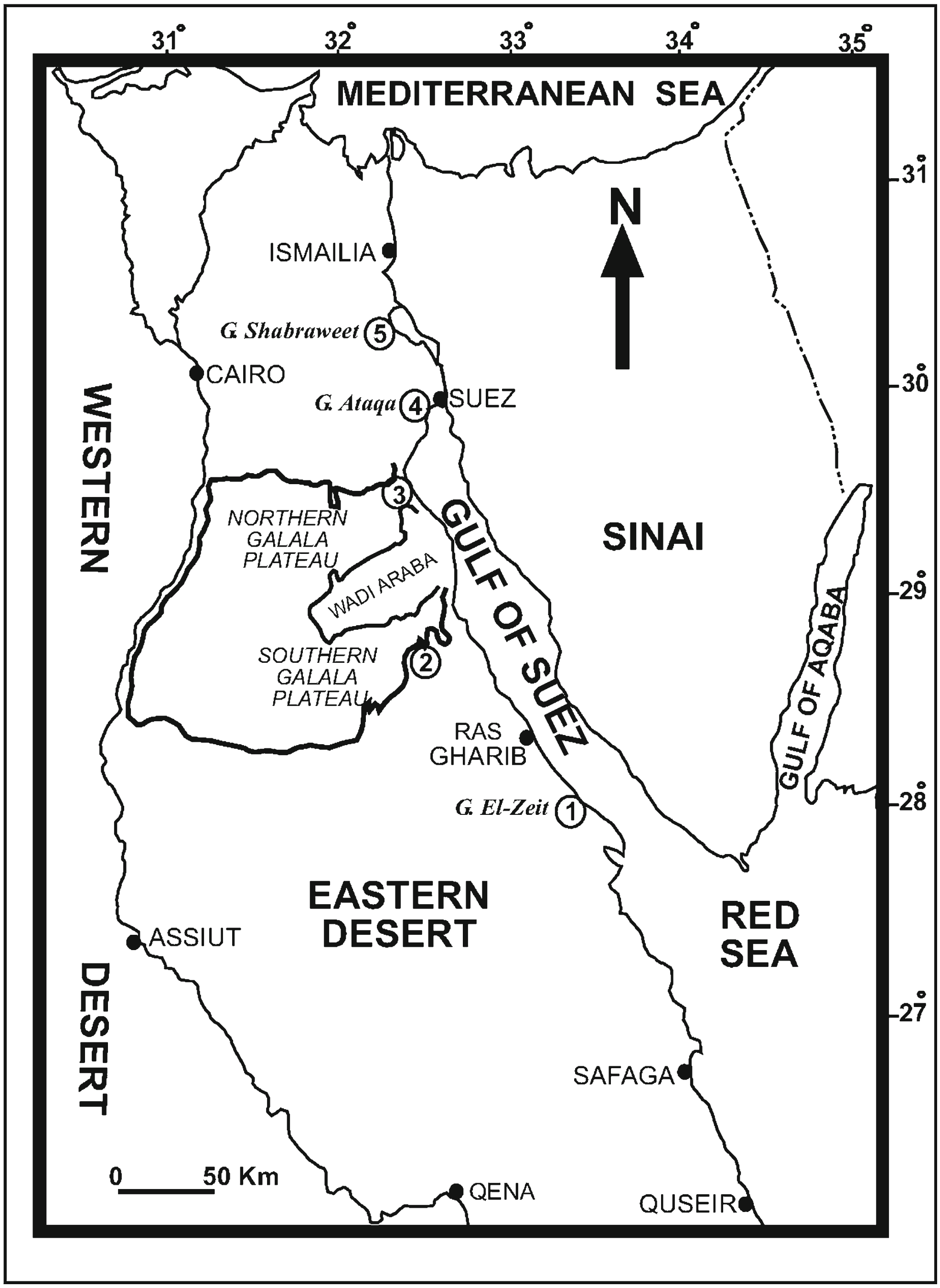

Fig. 1 Location of the studied sections

of Rh-target tube, LiF-420 crystal, gas flow proportional counter, coarse collimators, vacuum, 70 kV and 15 mA, for Sr. A chemical analysis (XRF and normal wet-chemical techniques) of 20 powdered rock samples for their major oxides (CaO, MgO, Fe_2O_3, and Al_2O_3) and trace elements (Sr and Na) were carried out in order to throw some light on the chemical characteristics of the studied rocks. (e) Twenty-seven carbonate rocks were micro-sampled for oxygen and carbon isotopic analyses in order to discuss the origin of dolostones and the cements. The analyses were carried out at the laboratory of stable isotope at the University of Windsor, Canada using a microscope-mounted drill assembly to extract the desired quantity (2–5 mg) of powdered samples from polished slabs. The samples for isotope analysis (n=28) were reacted in vacuum with 100 % pure phosphoric acid for at least 4 h at 25 °C for calcite and 50 °C for dolomite using the method described by Al-Aasm et al. (1990). The developed CO_2 gas was analyzed for isotopic ratios on a Delta plus mass spectrometer. Values of O and C isotopes are reported in per mil (‰) relative to the Pee Dee Belemnite (VPDB) standard and were corrected for phosphoric acid fractionation. Precision was better than 0.05 ‰ for both $\delta^{18}O$ and $\delta\ ^{13}C$.

Carbonate diagenesis

The carbonate digenesis of the Galala Formation was developed in the following four main diagenetic environments: marine–phreatic, mixed marine–meteoric, meteoric–phreatic, and subaerial environments. The carbonate diagenetic processes and their related diagenetic environments are summarized in Fig. 2.

Marine–phreatic diagenesis

Micritization

Micritization causes the transformation of the skeletal allochems into dark, structureless, and homogeneous masses of blindly massive micrite. It is well represented in the peloidal–algal–skeletal wackestones, skeletal packstones, and grainstones of the Southern and Northern Galalas and Gebel Shabraweet. Most of the skeletal constituents have been subjected with partial to complete micritization. Although the algal bioclasts are the most affected grains, also the molluscs,

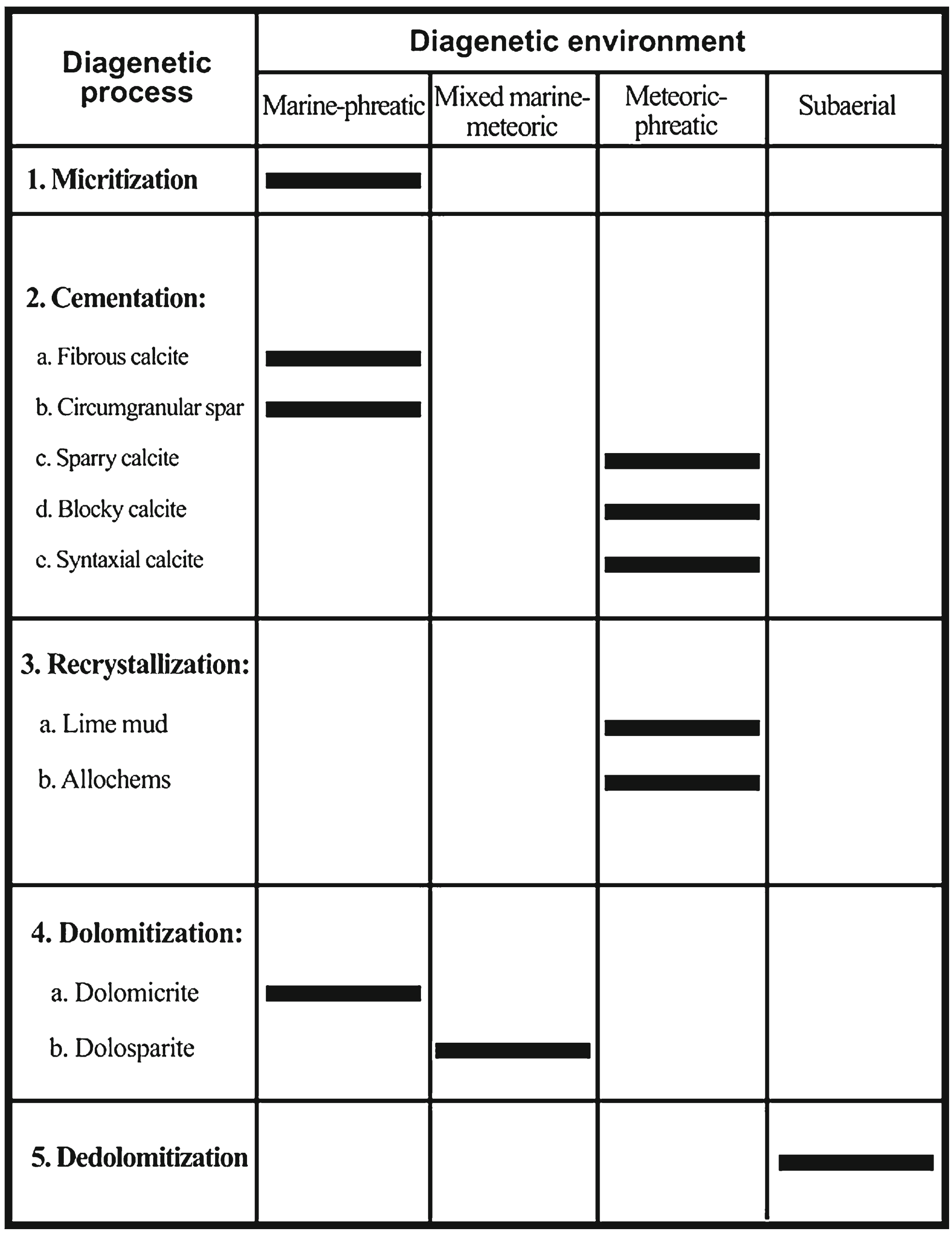

Fig. 2 The main carbonate diagenetic processes and their link to diagenetic environments

echinoderms, benthic foraminifera, and oolites allochems are affected by this process with variable degrees (Fig. 3a, b). Partial micritization results in creating micritic envelopes around the mollusc shell debris and echinoid spines and stems (Fig. 3c). Also, it is noticed that many pores and cavities surround the rims of the micritized allochems (Fig. 3d).

Marine cementation

Fibrous cement It is the first generation of marine cement in the diagenetic history of the Galala Formation. It was identified from the Southern and Northern Galalas and Gebel Shabraweet. It is represented by thin, closely packed fringes

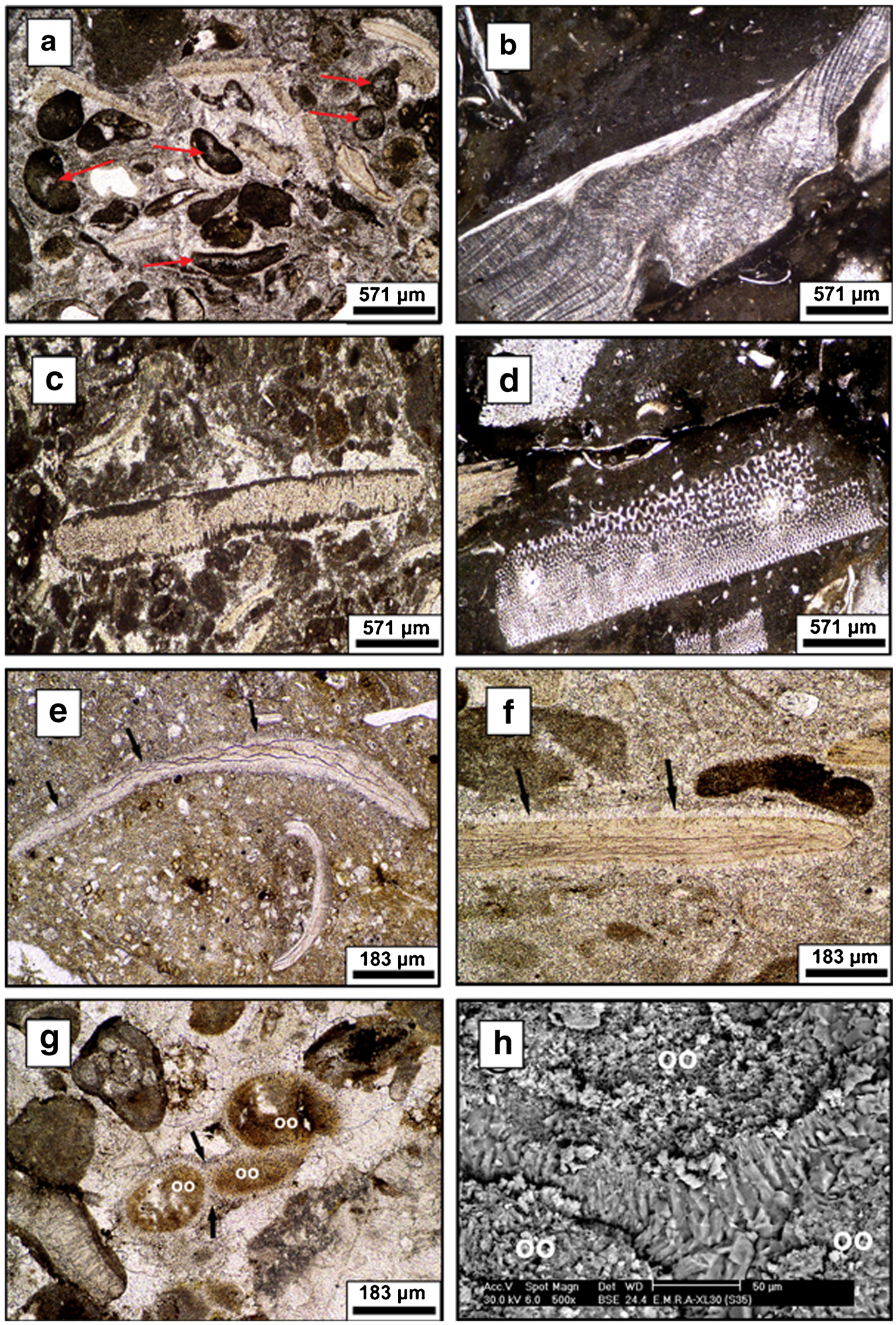

Fig. 3 **a** Thin-section phptomicrograph shows the micritization of algae (*red arrows*), Gebel Shabraweet, O.L. **b** Thin-section phptomicrograph shows the micritization of a bivalve bioclast, the Northern Galala, O.L. **c** Thin-section phptomicrograph shows a micrite envelope around the exterior of an echinodermal bioclast, Gebel Shabraweet, O.L. **d** Thin-section photomicrograph explaining the phases of the micritization process. *1* Perforation of a bivalve particle by the encrusting algae leads to forming of microborings that are filled with micrite. *2* The repeating boring and infilling of the micoborings with microcrystalline precipitates results in transformation of the particle into a mass of micrite (peloid). The Northern Galala. O.L. **e**. Thin-section photomicrograph showing the fibrous calcite rim cement around a bivalve bioclast (*arrows*). Such cement is composed of tightly packed, fibrous to bladed calcite crystals oriented with their long axes normal or nearly normal to the surface of the bivalvian particle. The Northern Galala, O.L. **f** Thin-section photomicrograph showing circumgranular spar cement (*arrows*) around a bivalve allochem. Molluscan peloidal packstone. Gebel Shabraweet, O.L. **g** Circumgranular spar cement (*arrows*) enveloping ooids (oo), Gebel Shabraweet, O.L. **h** SEM image showing the polygonal boundaries of the circumgranular spar cement between the ooids (oo), Gebel Shabraweet

of semi-opaque fibrous calcite grow perpendicular to the outer boundaries of some bivalve shells (Fig. 3e). Such crystals are mostly exhibiting straight or planar contacts with each other. The length of these fibrous crystals ranges from 4 to 7 μm.

Circumgranular spar cement The circumgranular spar represents the second generation of the marine–phreatic cements. It was identified from the Northern Galala, Gebel Ataqa, and Gebel Shabraweet. The best-developed circumgranular cement was observed from the grainstones (oolitic peloidal and peloidal echinoi dal grainstones) of Gebel Shabraweet; whereas, the circumgranular cement borders the outer margins of both ooids and peloids. The circumgranular calcite cement is represented herein by fine-crystalline spar (average=50 μm) with clear to cloudy appearance arranged normal or nearly normal to the outer margin of the allochemical constituents and with a length to width ratio between 1:1 and 2:1. In spite of the boundaries between the circumgranular crystals are often planar (Fig. 3f, g), polygonal boundaries of circumgranular cement were observed in some rocks (Fig. 3h).

Dolomitization

The dolomitization is the most prominent diagenetic process of the Galala Formation. It is more extensive at the northern part of the study area (Gebel Ataqa and Gebel Shabraweet). Two phases of dolomititization are recognized; early and late diagenetic. Since the distinction between the calcite and dolomite in partially dolomitizied rocks is very difficult, this study concentrates on the pervasive dolomitization (dolomicrites and dolosparites).

Early diagenetic dolostone (dolomicrite)

Petrography The early diagenetic dolomitization results in the formation of fine-crystalline dolostone (dolomicrite). The fine-crystalline dolostone includes six lithofacies: dolomicrite, sandy dolomicrite, sandy glauconitic dolomicrite, birds eye dolomicrite, ferroan dolomicrite, and siliceous ferroan dolomicrite. The dolomicrite is composed of fine (4 to 40 μ), idiotopic to xenotopic, interlocking mosaics associated with gypsum (Figs. 5h and 6a–c). Biogenic sedimentary structures are represented by burrowing and birds eyes.

Geochemistry Thirteen representative samples of dolomicrite were geochemically analyzed in order to determine the stoichiometry, major oxides (CaO, MgO, Fe_2O_3, and Al_2O_3) and trace elements (Sr and Na) (Table 4). Three of these samples represent sequence boundaries; hence, they show the totally different values of chemical composition. The dolomicrite has an average value of 30.89 wt% for CaO and 17.12 wt% for MgO. It is non-stoichiometric Ca-rich since the average $CaCO_{3\ (mol\%)}$ is 55.13 and the average $MgCO_{3\ (mol\%)}$ is 35.79. Fe_2O_3 has a low wt% (1.12–3.45 %), while Al_2O_3 wt% ranges from 1.7 % to 8.6 %. Sr content ranges from 512 to 717 ppm (average=603 ppm), while Na values are ranging from 1,005 to 2,680 ppm (average=1,694 ppm).

Stable isotope analysis Ten representative samples of dolomicrite were analyzed for their stable isotope composition ($\delta^{18}O$ and $\delta^{13}C$). All values of $\delta^{18}O$ are >−2 VPDB‰ (0.95 to −1.7 VPDB‰ with average=−0.76‰; Table 4). The $\delta^{13}C$ values of the studied dolomicrite range from 2.8 to −1.74 VPDB‰ (average=0.933‰; Table 4). The $\delta^{18}O$ versus $\delta^{13}C$ values of the studied dolomicrite are plotted in Fig. 7.

Late diagenetic dolostone (dolosparite)

Petrography The late diagenetic dolomitization causes the formation of coarse-crystalline dolostone (dolosparite). The dolosparite is composed of dolomite rhombs ranging in size from 40 to 220 μm with pronounced intercrystalline porosity and sucrosic equigranular fabric (Fig. 6d). The majority of the dolomite rhombs exhibits well-developed zoning.

Geochemistry Seven dolosparite samples were subjected to geochemical analysis. The average wt% of CaO and MgO of the dolosparite are 29.1 % and 15.8 %, respectively. The dolosparite is non-stoichiometric; whereas, the average $CaCO_{3\ (mol\%)}$ and $MgCO_{3\ (mol\%)}$ are 52 and 33, respectively. The Fe_2O_3 is not detected in four samples, while it reaches its maximum percentage (3.8 %) in the dolosparite of Gebel El-Zeit. The Al_2O_3 ranges from 2.26 % to 7.88 % (Table 4). Sr values are ranging from 133 to 244 ppm (average=199 ppm), while Na values are ranging from 244 to 441 ppm (average=389 ppm).

Stable isotope analysis The $\delta^{18}O$ of dolosparite are showing more negative values (−4.01 to −2 VPDB‰) than those of dolomicrite (0.95 to −1.7 VPDB‰; Table 4). The $\delta^{13}C$ values of dolosparite range from 1.5 to 2.87 VPDB‰. This, besides the lack in fossils, suggests that the dolosparite is produced from non-biogenic carbonate-rich water.

Meteoric–phreatic diagenesis

Meteoric cementation

Granular sparry calcite cement The granular sparry calcite cement of the Galala Formation occurs in three different textural positions. The first is intergranular precipitates; occluding the pore spaces between the allochems of the grainstones of Gebel Shabraweet (Fig. 5a). The absence of any relics of dark micrite reflects that it is cement not a neomorphic spar. The $\delta^{18}O_{VPDB}$‰ of the interparticle sparry calcite cement in the oolitic peloidal grainstone of Gebel

Table 3 Oxygen and Carbon isotopic values of representative limestone and dolostone samples

Studied section	Bed no.	Facies name	Notes	δ^{13}C VPDB‰	δ^{18}O VPDB‰
Gebel Shabraweet	33	Oolitic peloidal grainstone	Granular sparry calcite cement	1.49	−4.93
Gebel Ataqa	57	Birds eye dolomicrite	Sparry calcite cement fills birds eyes	0.92	−1.98
Southern Galala	28	Oncolitic packstone	Neomorphic spar	0.17	−5.17
Northern Galala	82	Ostracoda molluscan packstone	Neomorphic spar	1.02	−4.96
Gebel Shabraweet	100	Molluscan-echinoidal wackestone	Neomorphic spar	1.23	−4.83
Gebel El-Zeit	124	Rooted ferr. Sublitharenite	Caliche	1.61	−5.72
Northern Galala	83	Claystone	Caliche	−3.38	−11.91

Shabraweet is −4.93‰ and the $\delta^{13}C_{VPDB}$‰ value is 1.49‰ (Table 3 and Fig. 4). The second type fills partially or completely the cavities and internal hollows of the dissolved bioclasts (biomouldic porosity; Fig. 5b). These intragranular sparry calcites are usually inclusion-free and are sometimes well-edged. They grow coarser towards the center of the leached bioclast, and hence, they exhibit drusy calcite mosaics. The third type is the void or cavity fillings (birds eye structures in some dolostones of the Gebel Ataqa and the Northern Galala). Such calcites are limpid with euhedral to subhedral contacts (Fig. 5c). The $\delta^{13}C_{VPDB}$‰ value of the birds eye calcite is 0.92, while the $\delta^{18}O_{VPDB}$‰ value is −1.98 (Table 3 and Fig. 4).

Blocky calcite cement It is a common cement filling of the intraparticle pores, fractures, and intergranular pore spaces in the lime mudstone of the basal part of both Gebel El-Zeit and Gebel Ataqa and in the dolomicrite of the basal part of Gebel Shabraweet. It is composed of limpid to translucent euhedral crystals with an average size of 600 μm, displaying a sharp contact relationship with the surroundings microsparry calcite (Fig. 5d).

Syntaxial overgrowth cement It is a continuous to discontinuous clear cement that surrounds almost all the echinoderm fragments of the Southern and Northern Galalas and Gebel Shabraweet (Fig. 5e).

Recryatallization

Aggrading neomorphism of lime–mud matrix The aggrading neomorphism of lime–mud matrix is a common process in the diagenetic history of the Galala Formation. It is recognized from the majority of the studied lime mudstones, wackestones, and packstones with variable degrees. The lime–mud matrix in between allochems is partially neomorphosed into patches of microsparites in the earlier stages of neomorphism (15–35 μm) and into pseudosparites (average=75 μm) during the more advanced stages of neomorphism. The neomorphosed spar is inclusion-rich with turbid appearance providing anhedral form with non-planar to irregular boundaries (Fig. 5f).

The isotopic analysis of neomorphosed spar of representative wackestone and packestone from the Southern and Northern Galalas and Gebel Shabraweet displays a light

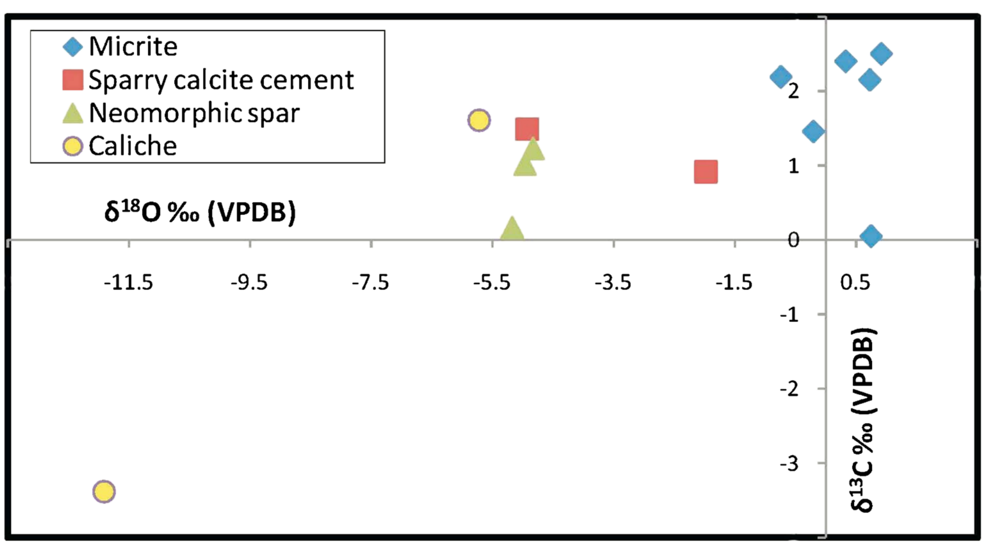

Fig. 4 Cross-plot of oxygen and carbon isotopic composition of representative phases in limestone and dolostone microsamples

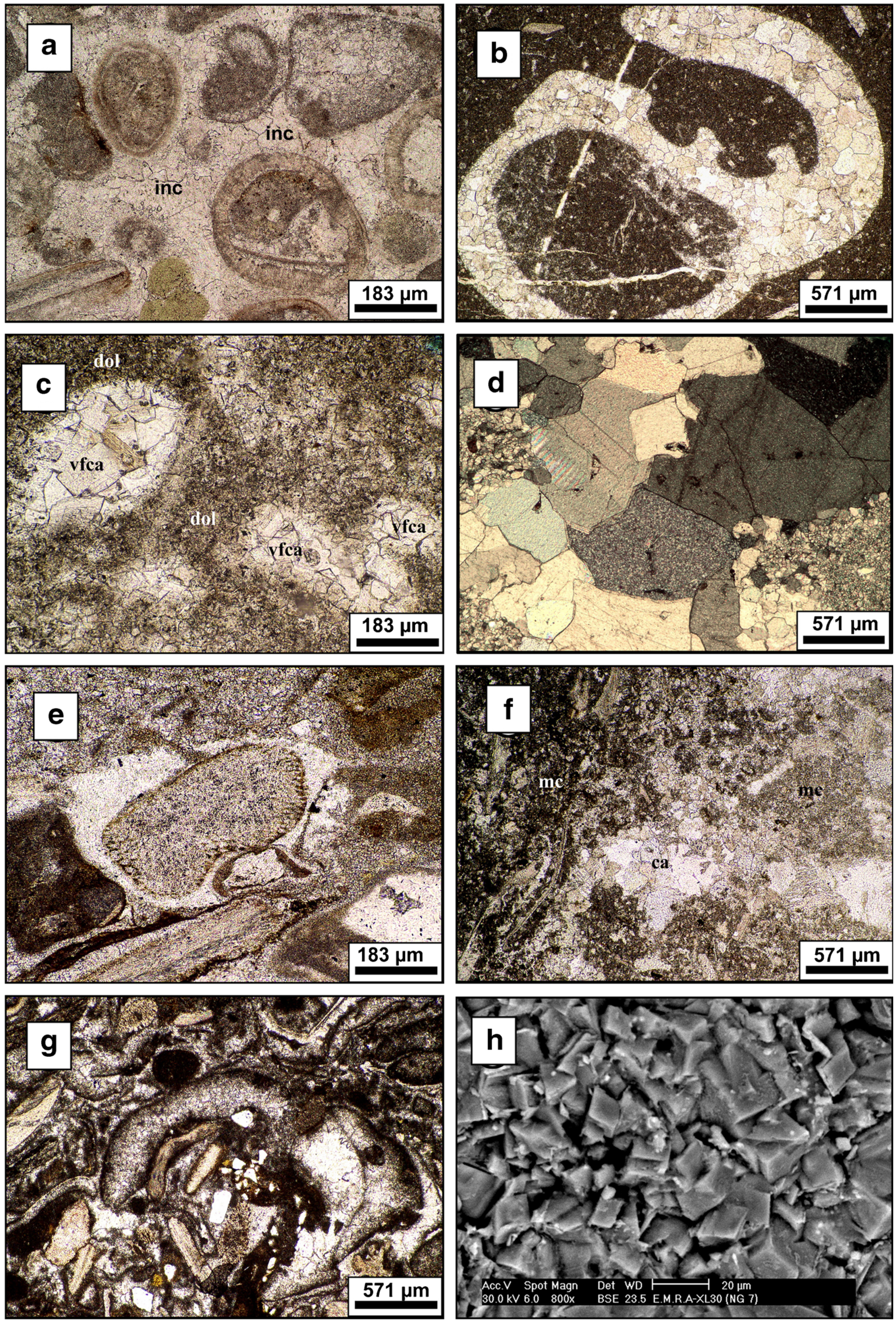

Fig. 5 **a** Intergranular sparry calcite cement (inc) between peloids and ooids, Gebel Shabraweet, O.L. **b** Infilling of cavities of gastropod by granular sparry calcite cement, the Southern Galala, O.L. **c** Void-filling calcite cement (vfca) filling the internal structure of birds eyes surrounded by dolomicritic matrix (dol), Gebel Ataqa, O.L. **d** Blocky calcite cement filling a cavity in lime mudstone, Gebel El-Zeit, C.N. **e** Syntaxial calcite rim cement around an echinoderm, Gebel Shabraweet, C.N. **f** Aggrading neomorphism of lime mud. Notice: the co-existence of micro- and pseudospars (ca) and the dark un-neomorphosed micrite patches (mc), Gebel Ataqa, O.L. **g** Bivalve shells have undergone calcitization from their center to peripheries, Gebel Shabraweet, O.L. **h** SEM image showing a general picture of the planar, hypidiotopic to idiotopic dolomicrite, the Northern Galala

$\delta^{13}C_{VPDB}$‰ values (0.17 to 1.23‰) with the average value= 0.8‰ and depleted $\delta^{18}O_{VPDB}$‰ (−4.96 to −5.17‰) with the average value=−4.98‰. The $\delta^{13}C_{VPDB}$‰ value of the caliche of the uppermost Gebel El-Zeit is 1.61‰ and that of the caliche of the Northern Galala is −3.38. The $\delta^{18}O_{VPDB}$‰ of the caliche of the uppermost Gebel El-Zeit is −5.72‰, while that of the caliche of the Northern Galala is −11.91‰ (Table 3 and Fig. 4).

Calcitization of skeletal particles It is a stabilization process by which the aragonite and high Mg-calcite that build up the original structure of some allochems are converted into Mg-depleted calcite under the influence of t meteoric water (Chaftez et al. 1988). The intensity of calcitization varies from the low-degree, incomplete to the high-degree, intensive calcitization. The resulted calcite crystals are easily distinguished by their turbid appearance, wavy to irregular boundaries, and patchy fabric due to the variability in the distribution of the crystal size. It is noticed that the bivalve bioclasts are the most extensively calcitized skeletal particles (Fig. 5g).

Dedolomitization

The dedolomitization process is infrequently recorded in the Gebel El-Zeit, Northern Galala, Gebel Ataqa, and Gebel Shabraweet; whereas, it is portrayed by the partial calcitization of the precursor dolomites. Such calcitized dolostones were distinguished in the field by their mottling appearance (lighter color within the dark gray unreplaced dolostone). The petrographic investigation on stained thin sections shows that the dedolomitization is represented by well-developed dolomites engulfed in larger subhedral to anhedral, blocky to massive phenocrystals of calcite, exhibiting a poikilotopic texture (Fig. 6e). Sometimes, these calcites contain dark relics of the precursor, unreplaced dolomites. The calcitization of the dolomite rhombs is proceeding from their rims towards the centers proceeds from rims towards the centers (Fig. 6f).

It is observed that the dedolomites of the Galala Formation are always identified in the dolostones that are capping the shallowing–upward cycles. Also, the degree of dedolomitization increases near the sequence boundaries. Petrographically, it is noticed that the dedolomitization goes to be more intensive nearby the fissures and cracks.

Discussion

The micritization is the first diagenetic process in the diagenetic history of the Galala Formation (Fig. 2). It took place during or shortly after deposition in concomitant to or shortly before marine cementation (Khalifa 2005). The petrographic analysis elucidates that there are a lot of pores and cavities around the external margins of the micritized carbonate grains

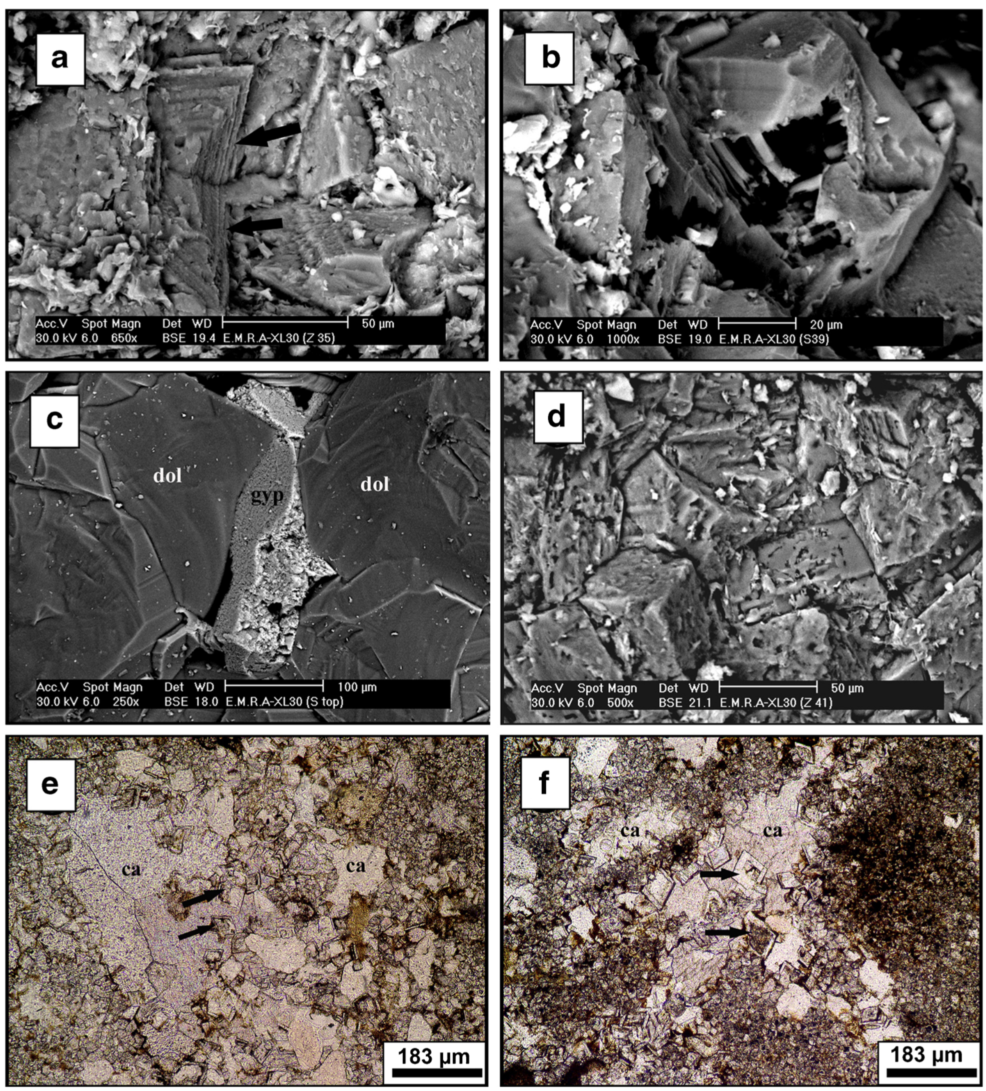

Fig. 6 **a** SEM image showing the dolomite overgrowths (*arrows*) around dolomite rhombs, Gebel El-Zeit. **b** SEM image showing dissolution of dolomite core, Gebel Shabraweet. **c** SEM image showing gypsum (gyp) in-between dolomite rhombs (dol) of the dolomicrite, Gebel Shabraweet. **d** SEM image showing a general picture of dolosparite, Gebel Ataqa. **e**, **f** The dedolomitization process; the idiotopic dolomite rhombs are engulfed by blocky to massive calcite crystals (ca) showing poikilotopic texture, Gebel Shabraweet, O.L

Table 4 Geochemical and isotopic data of representative dolostone samples (dolomicrite and dolosparite)

Studied section	Bed no.	Lithofacies	CaO %	$CaCO_3$ (Mole%)	MgO%	$MgCO_3$ (Mole%)	Fe_2O_3%	Al_2O_3%	Na (ppm)	Sr (ppm)	$\delta^{13}C$ VPDB‰	$\delta^{18}O$ VPDB‰
Gebel Shabraweet	10	Dolomicrite	30.3	54.08	20.11	42.03	nd	1.7	2,680	618	–	–
Gebel Shabraweet	31	Dolomicrite	28.1	50.1	18.1	37.8	2.1	3.69	2,019	550	2.77	−1.09
Gebel Shabraweet	39	Dolomicrite	32.3	57.65	21.12	44.32	nd	3.7	1,030	654	0.4	0.95
Gebel Shabraweet	42	Dolomicrite	34.4	61.4	13.1	27.4	1.12	4.6	1,308	533	–	–
Northern Galala	7	Dolomicrite	30.1	53.72	16	33.44	1.4	5.9	1,801	696	0.24	−0.44
Northern Galala	9	Dolomicrite	29.4	52.47	17.5	36.57	1.12	8.6	1,474	548	1.14	−1.47
Northern Galala	44	Dolomicrite	29.6	52.83	17.5	36.57	nd	8.3	2,011	512	2.47	−1.24
Gebel Ataqa	29	Dolomicrite	31.65	56.49	19.61	40.98	1.9	3.33	1,005	653	2.8	−0.36
Gebel Ataqa	38	Dolomicrite	31.4	56.04	16.5	34.48	nd	2.51	2,480	717	0.8	−0.14
Gebel Ataqa	59	Dolomicrite	29.2	52.12	16.2	33.85	2.6	3.6	1,133	549	1.13	−0.88
Northern Galala (SBNG.2)	25	Dolomicrite	33.54	59.86	16.88	35.27	2.56	4.59	244	164	–	–
Northern Galala (SBNG.4)	58	Dolomicrite	32.33	57.7	14.71	30.74	1.62	2.56	375	137	–	–
Gebel Ataqa (SBA.4)	61	Birds eye dolomicrite	29.31	52.31	15.23	31.83	3.45	3.18	274	183	–	–
Gebel El-Zeit	15	Ferroan dolomicrite	–	–	–	–	–	–	–	–	−1.74	−1.29
Gebel El-Zeit	52	Sandy dolomicrite	–	–	–	–	–	–	–	–	−0.68	−1.7
Gebel El-Zeit	78	Dolosparite	29.11	51.96	14.82	30.9	2.2	5.5	244	133	1.5	−2.99
Gebel El-Zeit	80	Dolosparite	26.2	46.76	13.72	28.67	nd	7.88	408	242	–	–
Gebel El-Zeit	84	Dolosparite	26.33	46.99	15.38	32.14	3.8	5.28	396	167	–	–
Gebel Ataqa	48	Dolosparite	32	57.12	15.4	32.18	nd	3.02	441	178	2.87	−4.01
Gebel Shabraweet	42	Dolosparite	31	55.33	16.4	34.27	nd	4.28	389	244	–	–
Gebel Shabraweet	102	Dolosparite	28.41	50.71	16.2	33.85	1.61	6.5	440	210	2.55	−2
Gebel Shabraweet	118	Dolosparite	30.9	55.15	19	39.71	nd	2.26	407	218	1.79	−3.26

(*nd* not detected)

(Fig. 3d). Consequently, the role of encrusting algae (Bathrust 1975; Harris et al. 1979; May and Perkins 1979) is adopted herein to interpret the micritization process. The grains are cemented by fibrous and circumgranular cements, respectively, in the marine–phreatic diagenetic environment shortly after micritization (Fig. 2). Many authors described and interpreted such cements from the shallow marine–phreatic diagenetic environment (e.g., James and Choquette 1983; Tucker 1993; Melim et al. 2002).

Contemporaneously, the lime mud is subjected to pervasive dolomitization to yield fine-crystalline dolostone (dolomicrite; Fig. 2). The size and fabric of the studied dolomicrite resemble the penecontemporaneous dolostone of the ancient and recent supratidal–intertidal flats. The penecontemporaneous dolomite (<40 μm) is formed in early phase of dolomitization by replacing the lime mud shortly after the sedimentation of the carbonate minerals (Lee and Friedman 1987 and Amthor and Friedman 1991). The low Fe content (1.12–3.45 %) of the dolomicrite reflects that it has been formed in a near-surface oxidizing environment characteristic of carbonate ramps (Land 1985). The high wt% of Al_2O_3 (1.7 % to 8.6 %) in comparison with the Fe_2O_3 is attributed to the high content of claystones forming the basal parts of cycles (Table 4). Sr content of the investigated dolomicrites is ranging from 512 to 717 ppm with average=603 ppm, while Na content is ranging from 1,005 to 2,680 ppm with the average value=1,694 ppm (Table 4). Such values fall within the range of the hypersaline to marine dolomite (Morrow 1988). The hypersaline–marine dolomite contains Sr content ranges from 500 to 900 ppm (Mitchel et al. 1987 and Wanas 2002). The Na concentration of the marine dolomite ranges from 1,000 to 3,000 ppm (Land and Hoops 1973). The $\delta^{18}O$ values of the dolomicrite of the Galala Formation (0.95 to −1.7 VPDB‰ with average=−0.76‰; Table 4) are compatible with that of the marine ancient dolomite, which range from +2.4 to −2.5 VPDB‰ (Moss and Tucker 1995; Holail et al. 1997; Railsback and Hood 2001). The deviation of the $\delta^{18}O$ to the negative values suggests that the dolomicrite of the Galala Formation was influenced by later fluids (Lonnee and Al-Aasm 2000). The $\delta^{13}C$ values (2.8 to −1.74 VPDB‰ with average=0.933‰; Table 4) support the marine origin of the fine-crystalline dolostone (Irwin et al. 1977). The cross-plot diagram of $\delta^{18}O$ versus $\delta^{13}C$ values of dolomicrite indicates that they fall within the zone of marine dolomite (Al-Aasm and Veizer 1986; Major et al. 1992; Fig. 7).

The admixture of meteoric water with marine water due to sea-level fall favors the aggrading recrystallization of the fine-crystalline dolomite (dolomicrite) into coarse-crystalline dolomite (dolosparite) (Fig. 2). The neomorphic origin of dolosparite can be evidenced by the presence of relics of finer dolomite within the coarser one and the variation from euhedral to anhedral dolomite crystals. Such polymodal size distribution may be ascribed to the neomorphic alteration and/or the heterogeneous grain size distribution of the precursor limestones and/or dolomicrite. The depleted Sr content of studied dolosparite (133 to 244 ppm with the average value=199 ppm) indicates that the dolomitization process has taken place in a mixed marine–meteoric water (Table 4). The Sr content of the mixing marine–meteoric dolomites ranges from 100 to 250 ppm (Supko 1977). It is granted that the Sr content of dolostone decreases with the increase of the extent of recrystallization by meteoric water (Nielsen et al. 1994 and Al-Hodairi and El-Hadad 1997). The Na values of dolosparite of the Galala Formation (244 to 441 ppm with average value 389 ppm; Table 4) indicate that it was originated in a mixed saline–meteoric waters (Badiozamani 1973; Loukina and Abu El-Anwar 1994). The low Na content (200–500 ppm) was attributed to the mixing marine–meteoric dolostones (Sibley 1980). The $\delta^{18}O$ values of the examined dolosparite ranges from −4.01 to −2 VPDB‰ (Table 4). This suggests that it was originated by a fluid of salinity less than that of the seawater. Also, it can be formed by an increase in temperature due to the burial effect. The average value of $\delta^{18}O$ of dolosparite is −3‰, which reflects depletion in oxygen. This suggests that it is

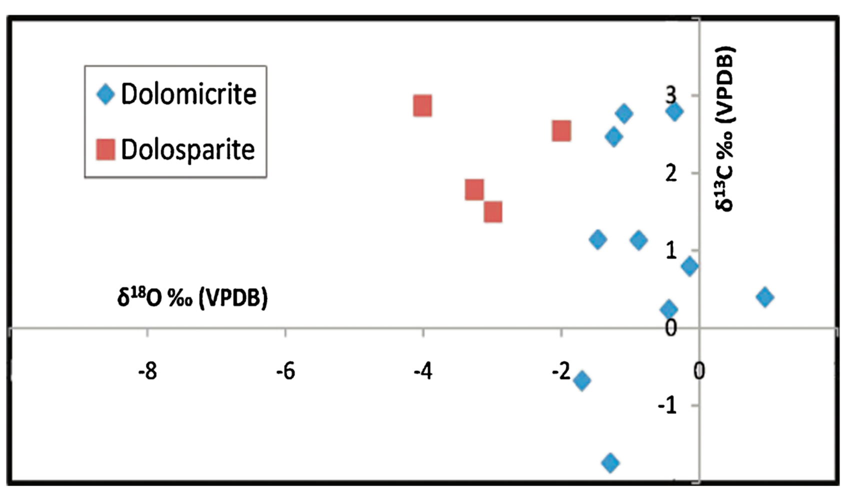

Fig. 7 Cross-plot of oxygen and carbon isotopic composition of representative dolostone bulk samples (dolomicrite and dolosparite)

originated by the mixing of meteoric and marine waters that promote aggrading neomorphism of the early dolomite (dolomicrite; Khalil 1999). The cross-plot diagram of $\delta^{18}O$ versus $\delta^{13}C$ (Fig. 7) displays that the investigated dolosparite is located within the mixed marine–meteoric, coarse-crystalline dolostones of the Upper Cretaceous Bahariya, Egypt (Holail et al. 1988) and of the Asmari Formation, SW Iran (Ranjbaran et al. 2007).

More severe sea-level fall results in the cementation of the carbonate particles by granular sparry calcite, blocky calcite, and the precipitation of the syntaxial overgrowth around the echinoidal particles in the meteoric water diagenetic environment (Fig. 2). The light $\delta^{18}O_{VPDB}$‰ (−4.93‰) of the studied interparticle sparry calcite cement indicates that it was precipitated in the meteoric-influenced pore waters (Holail et al. 1997; Fig. 4 and Table 3). Sun (1990) concluded that the intergranular cement in the biosparites is precipitated from the meteoric fluids. The $\delta^{13}C_{VPDB}$‰ (0.92) and $\delta^{18}O_{VPDB}$‰ (−1.98) values of the granular calcite cement within the birds eyes are indicative of diagenesis in the meteoric pore waters (Maliva 1995; Fig. 4 and Table 3). The common fossil-leaching feature indicates an active water circulation of the meteoric–phreatic zone (Tucker and Wright 1990). The sparry calcite cement is inferred to have precipitated as a low Mg-calcite cement in the meteoric–phreatic diagenetic environment (Moore 1989; Essa 2005). The blocky calcite cement filling the intraparticle voids, fractures, and pore spaces was interpreted to have been precipitated in the meteoric–phreatic zone by James and Choquette (1990) and Vincent et al. (2007). The syntaxial overgrowth cement is interpreted to be formed in the meteoric–phreatic diagenetic environment by many authors; among them were Heckel (1983) and Harris et al. (1997).

Meteoric cementation is followed by the recrystallization process (Fig. 2). Recrystallization affects both the lime–mud matrix (aggrading neomorphism into micro- and pseudosparites) and the skeletal allochems (stabilization or calcitization). The chemical instability of the aragonite and high Mg-calcite is the driving force for the aggrading neomorphism. The present authors believe that the clay minerals and/or argillaceous material is responsible for the aggrading neomorphism of the lime–mud matrix as they adsorb the Mg^{2+} ions that obstruct the growth of the micrite and hence favor the aggradational growth of the micrite into coarser neomorphic spar. Similar examples were elucidated by Folk (1974), Khalifa and Zaghloul (1990), and Abu El-Ghar and Hussein (2005). The light $\delta^{13}C_{VPDB}$‰ (0.17 to 1.23‰) and depleted $\delta^{18}O_{VPDB}$‰ (−4.96 to −5.17‰) isotopic values of the studied neomorphosed spar indicate a meteoric diagenetic environment (Holail et al. 1997; Fig. 4 and Table 3). The aggrading neomorphism of lime mud takes place in meteoric–phreatic environment (Flügel 1982; Harris et al. 1997). Many authors believe that the calcitization process goes on when the skeletal allochems are subjected to meteoric water, resulting in the replacement of these shells by the more stable neomorphic spar (e.g., Ahmad et al. 2006 and Knoerich and Mutti 2006).

Some dolostones are exposed to dedolomitization (calcitization) during the subaerial exposure and weathering periods. This results in formation of calcite at the expense of dolomite. The meteoric water mechanism is proposed herein to interpret the dedolomitization process; whereas, the percolation of the meteoric water on the exposed surface of dolostones or through the fissures and cracks leads to the removal of Mg and the formation of calcite. This interpretation goes in harmony with the opinions of Folkman (1969) and Braun and Friedman (1969).

References

Abu El-Ghar MS, Hussein AW (2005) Post-depositional changes of the Lower-Middle Eocene limestones of the area between Assiut and Minia, West of the Nile Valley, Egypt. 1st Inter Conf Geol Tethys Cairo Univ: 229–248

Abu El-Hassan MM (1997) Geochemistry and diagenesis of the Cenomanian dolomite at Gebel Shabraweet and Arif El Naga area, Egypt. 3rd Conf Geochem Alex Univ 2(3-4):25–39

Ahmad AHM, Bhat GM, Khan MHA (2006) Depositional environments and diagenesis of the Kuldar and Keera Dome carbonates (Late Bathonian-Early Collovian) of western India. J Asian Earth Sci 27: 765–778

Al-Aasm IS, Veizer J (1986) Diagenetic stabilization of aragonite and low Mg calcite, 2. Stable isotopes in rudists. J Sed Pet 56:763–770

Al-Aasm IS, Taylor BE, South B (1990) Stable isotope analysis of multiple carbonate samples using selective acid extraction. Chem Geol 80:119–125

Al-Hodairi A, El-Hadad A (1997) Dolomitization of the Late Triassic-Early Jurassic Azizia Formation, Jebel Nafwa, NW Libya. 3rd Conf Geochem Alex Univ 2(3-4):57–67

Amthor JE, Friedman GM (1991) Dolomite rock textures and secondary porosity development in Ellenburger Group carbonates (Lower Ordovician), West Texas and Southern New Mexico. Sedimentology 38:343–362

Badiozamani K (1973) The Dorag dolomitization model-application to the Middle Ordovician of Wisconsin. J Sed Pet 43(4):965–984

Bathrust RGC (1975) Carbonate sediments and their diagenesis, 2 Enlargedth edn. Elsevier Sci Pub Co, Amesterdam, 658 p

Braun M, Friedman GM (1969) Carbonate lithofacies and environments of the Tribes Hill Formation (Lower Ordovician) of the Mohawk Valley, New York. J Sed Pet 39:113–185

Chaftez HS, McIntosh AG, Rush PF (1988) Freshwater phreatic diagenesis in the marine realm of Recent Arabian Gulf carbonates. J Sed Pet 58(3):433–440

Dickson JAD (1966) Carbonate identification and genesis as revealed by staining. J Sed Pet 36:491–505

El-Reedy MW (1984) The general physical and chemical features and the pollution level of El-Sabahia-Sabhan-El Reqa Soil localities, state of Kuwait. Internal Report Environmental Protection Dept., Ministry of Pub Health-El Kuwait (part 1: chemical methods)

Essa MA (2005) Sedimentology and sequence stratigraphy of the Pre-Miocene sedimentary succession of Gabal Zeit, Southern Gulf of Suez, Egypt. 4th Inter Conf Geol Afr 2:541–573

Flügel E (1982) Microfacies analysis of limestones. Springer, Berlin, 633 p

Folk RL (1974) The natural history of crystalline $CaCO_3$: effects of Mg content and salinity. J Sed Pet 44(1):40–53

Folkman Y (1969) Diagenetic dedolomitization in the Albian-Cenomanian Yagur Formation on mount camel (Palestine). J Sed Pet 39:380–385

Harris PM, Halley RB, Lukas KJ (1979) Endolith microborings and their preservation in Holocene-Pleistocene (Bahama-Florida) ooids. Geology 7:216–220

Harris MK, Thayer PA, Amidon MB (1997) Sedimentology and depositional environments of Middle Eocene terrigenous-carbonate strata southwestern Atlantic Coastal Plain, U.S.A. Sed Geol 108:141–161

Heckel PH (1983) Diagenetic model for carbonate rocks in Mid-continent Pennsylvanian eustatic cyclothems. J Sed Pet 53:733–759

Holail HM, Lohmann KC, Sanderson I (1988) Dolomitization and dedolomitization of Upper Cretaceous carbonates, Bahariya Oasis, Egypt. In: Shukla V, Baler P (Eds), Sedimentology and geochemistry of dolostones. Soc Econ Paleon Minerol Spec Publ 43: 191–207

Holail HM, Shaaban MN, Rifai RI, Abd-Alla M (1997) Diagenesis and porosity development of Upper Jurassic carbonates, El-Maghara area, Northern Sinai, Egypt. 3rd Conf Geochem Alex Univ 2(3–4):85–106

Hussein AW (2010) Stratigraphical and sedimentological studies on the Cenomanian rocks (Galala Formation), North Eastern Desert, Egypt. Ph.D Thesis Fayoum Univ: 270 p

Irwin H, Curtis CD, Coleman M (1977) Isotopic evidence for the source of diagenetic carbonates formed during burial of organic rich sediments. Nature 269:209–213

Issawi B, Osman R (2000) Upper Cretaceous-Lower Tertiary platform-ramp environments in northern Egypt. 5th Conf Geol Arab World (GAW5) Cairo Univ: 1289–1308

James NP, Choquette PW (1983) Diagenesis 6, limestones, the sea floor diagenetic environment. Geol Can 10:62–179

James NP, Choquette PW (1990) Limestones—the meteoric diagenetic environment. In: Mcllreath IA, Morrow DW (eds) Diagenesis. Geol Assoc Canada, Ottawa, pp 35–74

Khalifa MA (2005) Lithofacies, diagenesis and cyclicity of the Lower Member of the Khuff Formation (Late Permian), Al Qasim Province, Saudi Arabia. J Asian Earth Sci 25:719–734

Khalifa MA, Zaghloul EA (1990) Diagenesis in the Esna and Farafra formations, Farafra Oasis, Western Desert. Egypt Annal Geol Surv XVI:223–227

Khalil M (1999) Sedimentological and stratigraphical studies of the Cretaceous of Northern Sinai and neighbouring, Egypt. Ph.D Thesis Assiut Univ: 371 p

Khalil M, Mostafa A (2001) Diagenesis and diagenetic processes in the view of sequence stratigraphy for the Aptian-Upper Eocene sequences of Shabraweet and Ataqa areas, Gulf of Suez, Egypt. Al-Azhar Bull Sci 12(1):215–242

Knoerich A, Mutti M (2006) Missing aragonitic biota and diagenetic evolution of heterozoan carbonates: A case study from the Oligo-Miocene of the central Mediterranean. J Sed Res 76:871–888

Land LS (1985) The origin of massive dolomite. J Geol Educ 33:112–125

Land LS, Hoops GK (1973) Sodium in carbonate sediments and rocks: a possible index to salinity of diagenetic solution. J Sed Pet 43:614–617

Lee YI, Friedman GM (1987) Deep-burial dolomitization in the Ordovicain Ellenburger Group carbonates, west Texas. J Sed Pet 57:544–561

Lonnee J, Al-Aasm IS (2000) Dolomitization and fluid evolution in the Middle Devonian Sulphur Point Formation, Rainbow South Field, Alberta: petrographic and geochemical evidence. Bull Can Pet Geol 48(3):262–283

Loukina S, Abu El-Anwar E (1994) Geochemistry of Gabal Ataqa dolostones. Geol J Egypt 38(1):141–156

Major R, Lloyd RM, Lucia FJ (1992) Oxygen isotope composition of Holocene formed in a humid hypersaline setting. Geology 20:586–588

Maliva RG (1995) Recurrent neomorphic and cement microtextures from different diagenetic environments, Quaternary to Late Neogene carbonates, Great Bahama bank. Sed Geol 97:1–7

May JA, Perkins RD (1979) Endolithic infestation of carbonate substrates below the sediment-water interface. J Sed Pet 49:357–377

Melim LA, Westphal H, Swart PK, Eberli GP, Munnecke A (2002) Questioning carbonate diagenetic paradigms, evidence from the Paleogene of the Bahamas. Marine Geol 185:27–53

Mitchel JT, Land LS, Misr DE (1987) Modern marine dolomite cement in a North Jamican fringing reef. Geology 1:557–560

Mohammad MH, Omran MA (1992) Diagenesis of the sedimentary sequence in Shabraweet area, Egypt. Bull Fac Sci Zagazig Univ 14(2):220–240

Moore CH (1989) Carbonate diagenesis and porosity. Developments in sedimentology, vol 46. Elseveier, Amesterdam, 338 p

Morrow DW (1988) Diagenesis. Dolomite-part 1: the chemistry of dolomitization and dolomite precipitation. Geol Sci Can Rep Ser 4:113–123

Moss JM, Tucker M (1995) Diagenesis of the Barremian-Aptian platform carbonates, the Urgonian Limestone Formation of SE France: near-surface and shallow-burial diagenesis. Sedimentology 42: 853–874

Mostafa A, Hassan AM (2003) Lithofacies, diagenesis and depositional history of the Cenomanian-Turonian sequence of Gabal El-Zeit area, Gulf of Suez, Egypt. 3rd Inter Conf Geol Afr 1:467–483

Nielsen P, Swennen R, Keepens E (1994) Multiple-step recrystallization within massive ancient dolomite units: an example from the Dinantian of Belgium. Sedimentology 41:567–584

Railsback LB, Hood EC (2001) A survey of multi-stage diagenesis and dolomitization of Jurassic limestone along a regional shelf to basin transect in the Aziz Valley, Central High Atlas Mountains, Morocco. Sed Geol 139:285–317

Ranjbaran M, Fayazi F, Al-Aasm I (2007) Sedimentological, depositional environment and sequence stratigraphy of the Asmari Formation (Oligocene-Lower Miocene), Gachsaran area, SW Iran. Carbonates Evaporites 22(2):135–148

Shapiro L, Brannock WW (1962) Rapid analysis of silicate, carbonate and phosphate rocks. U S Geol. Surv Bull 1144A: 56 p

Sibley DF (1980) Climate control of dolomitization Sereo Domi Formation (Paleocene). In: Concepts and model of dolomitization, (edited by Zenger, NA, Dunhum, JB, Ethington RL). Soc Econ Paleont Mineral Spec Pub 28: 247–258

Sun QS (1990) Facies-related diagenesis in a cyclic shallow marine sequence: the Corallian Group (Upper Jurassic) of the Dorset Coast, Southern England. J Sed Pet 60(1):42–52

Supko PR (1977) Subsurface dolomites, San Salvador, Bahamas. J Sed Pet 47:1063–1077

Tucker ME (1993) Carbonate diagenesis and sequence stratigraphy. Sed Rev 1:51–72

Tucker ME, Wright VP (1990) Carbonate sedimentology. Blackwell Sci Pub, Oxford, 482 p

Vincent B, Emmanuel L, Houel P, Loreau JP (2007) Geodynamic control on carbonate diagenesis: petrographic and isotopic investigation of the Upper Jurassic formations of the Paris Basin (France). Sed Geol 197:267–289

Wanas HA (2002) Petrography, geochemistry and primary origin of spheroidaL dolomite from the Upper Cretaceous/Lower Tertiary Maghra El-Bahari Formation at Gabal Ataqa, Northwest Gulf of Suez, Egypt. Sed Geol 151:211–224